Science
AAAS

Trapping Molecules on a Chip
Samuel A. Meek, *et al.*
Science **324**, 1699 (2009);
DOI: 10.1126/science.1175975

References and Notes

1. D. J. Cram, *Nature* **356**, 29 (1992).
2. D. M. Vriezema *et al.*, *Chem. Rev.* **105**, 1445 (2005).
3. L. R. MacGillivray, J. L. Atwood, *Angew. Chem. Int. Ed.* **38**, 1018 (1999).
4. J. M. Kang, G. Hilmersson, J. Santamaria, J. Rebek, *J. Am. Chem. Soc.* **120**, 3650 (1998).
5. M. Marty, Z. Clyde-Watson, L. J. Twyman, M. Nakash, J. K. M. Sanders, *Chem. Commun. (Camb.)* 2265 (1998).
6. C. J. Hastings, D. Fiedler, R. G. Bergman, K. N. Raymond, *J. Am. Chem. Soc.* **130**, 10977 (2008).
7. M. Yoshizawa, M. Tamura, M. Fujita, *Science* **312**, 251 (2006).
8. M. Yoshizawa, Y. Takeyama, T. Okano, M. Fujita, *J. Am. Chem. Soc.* **125**, 3243 (2003).
9. D. R. Benson, R. Valentekovich, F. Diederich, *Angew. Chem. Int. Ed. Engl.* **29**, 191 (1990).
10. M. Kuil, T. Soltner, P. van Leeuwen, J. N. H. Reek, *J. Am. Chem. Soc.* **128**, 11344 (2006).
11. M. D. Pluth, R. G. Bergman, K. N. Raymond, *Science* **316**, 85 (2007).
12. V. M. Dong, D. Fiedler, B. Carl, R. G. Bergman, K. N. Raymond, *J. Am. Chem. Soc.* **128**, 14464 (2006).
13. L. Trembleau, J. Rebek, *Science* **301**, 1219 (2003).
14. M. Yoshizawa, T. Kusukawa, M. Fujita, K. Yamaguchi, *J. Am. Chem. Soc.* **122**, 6311 (2000).
15. D. J. Cram, M. E. Tanner, R. Thomas, *Angew. Chem. Int. Ed. Engl.* **30**, 1024 (1991).
16. T. Iwasawa, R. J. Hooley, J. Rebek Jr., *Science* **317**, 493 (2007).
17. R. Warmuth, *Angew. Chem. Int. Ed. Engl.* **36**, 1347 (1997).
18. R. Warmuth, M. A. Marvel, *Angew. Chem. Int. Ed.* **39**, 1117 (2000).
19. F. S. Dainton, *Trans. Faraday Soc.* **43**, 244 (1947).
20. P. R. Lewis, C. Price, *Polymer (Guildf.)* **12**, 258 (1971).
21. P. Mal, D. Schultz, K. Beyeh, K. Rissanen, J. R. Nitschke, *Angew. Chem. Int. Ed.* **47**, 8297 (2008).
22. Materials and methods are available as supporting material on *Science* Online.
23. C. L. D. Gibb, B. C. Gibb, *J. Am. Chem. Soc.* **126**, 11408 (2004).
24. E. Botana, E. Da Silva, J. Benet-Buchholz, P. Ballester, J. de Mendoza, *Angew. Chem. Int. Ed.* **46**, 198 (2007).
25. D. E. C. Corbridge, E. J. Lowe, *Nature* **170**, 629 (1952).
26. A. P. Ginsberg, W. E. Lindsell, K. J. McCullough, C. R. Sprinkle, A. J. Welch, *J. Am. Chem. Soc.* **108**, 403 (1986).
27. M. Peruzzini *et al.*, *Eur. J. Inorg. Chem.* 931 (1999).
28. I. Krossing, L. Van Wullen, *Chem. Eur. J.* **8**, 700 (2002).
29. D. Ajami, J. Julius Rebek, *Angew. Chem. Int. Ed.* **47**, 6059 (2008).

30. This work was supported by the Walters-Kundert Charitable Trust, the Royal Society, the Marie Curie IIF scheme of the 7th European Union Framework Program (to P.M.), and the Academy of Finland (project 212588, to K.R.). The authors also thank D. S. Wright for helpful discussions and a gift of white phosphorus and J. K. M. Sanders for useful comments on the manuscript. Mass spectra were provided by the Engineering and Physical Sciences Research Council National Mass Spectrometry facility at Swansea. CCDC-727817 contains the supplementary crystallographic data for this paper. These data can be obtained free of charge from the Cambridge Crystallographic Data Centre via www.ccdc.cam.ac.uk/data_request/cif.

Supporting Online Material

www.sciencemag.org/cgi/content/full/324/5935/1697/DC1
Materials and Methods
Figs. S1 to S3
References

22 April 2009; accepted 1 June 2009
10.1126/science.1175313

Trapping Molecules on a Chip

Samuel A. Meek, Horst Conrad, Gerard Meijer*

Magnetic trapping of atoms on chips has recently become straightforward, but analogous trapping of molecules has proved to be challenging. We demonstrated trapping of carbon monoxide molecules above a chip using direct loading from a supersonic beam. Upon arrival above the chip, the molecules are confined in tubular electric field traps ~20 micrometers in diameter, centered 25 micrometers above the chip, that move with the molecular beam at a velocity of several hundred meters per second. An array of these miniaturized moving traps is brought to a standstill over a distance of only a few centimeters. After a certain holding time, the molecules are accelerated off the chip again for detection. This loading and detection methodology is applicable to a wide variety of polar molecules, enabling the creation of a gas-phase molecular laboratory on a chip.

The manipulation of atoms above a chip using magnetic fields produced by current-carrying wires is a mature field of research (*1*). This field was inspired by the notion that miniaturization of magnetic field structures enables the creation of large field gradients, i.e., large forces and steep potential wells for atoms. Modern microelectronics technology makes it possible to integrate the multiple tools underlying these experiments onto a compact surface area. Such atom chips have been used to demonstrate rapid Bose-Einstein condensation (*2*) and have found applications in matter-wave interferometry and in inertial and gravitational field sensing (*3*). Likewise, the engineering of miniaturized electric field structures holds great promise for the manipulation of polar molecules above a chip (*4*). The latter might enable, for instance, the implementation of proposed schemes of quantum computation that use polar molecules as qubits (*5*, *6*). Here, we experimentally demonstrate a method for loading and detecting molecules on a chip, adding to the recent advances in the taming of molecular beams (*7*).

A schematic of the experimental setup with an expanded view of the chip with the array of microelectrodes, all contained in a compact high-vacuum machine, is shown in Fig. 1. The chip consists of a total of 1254 equidistant 10-μm-wide gold electrodes with a 40-μm center-to-center distance deposited onto a glass substrate, forming a structure that is 5 cm long (micro resist technology GmbH). All electrodes extend over a central 4-mm region, whereas outside this region the electrodes extend alternately to the left or right and terminate at three different lengths. Via the square pads and the nickel wires that are connected to every third electrode on either side of the array, six different potentials are applied to the electrodes. These potentials are described by $\pm V_0[1 + \cos(2\pi\nu t + \phi_n)]$, with exclusively positive (or negative) potentials applied to a given side of the array. Within each polarity set, three different phases ϕ_n with a mutual phase difference of $\pm 2\pi/3$ are used. In this way, tubular minima of electric field strength are generated every 120 μm, and these minima move over the chip with a speed given by 120 μm × ν (in MHz) at a constant height of about 25 μm. The diameter of the tubular electric field minima is about 20 μm, and with V_0 = 80 V, their depth is about 4 kV/cm. The two ends of the 4-mm-long tubular minima are closed in the present design by the fringe fields near the ends of the electrodes. A detailed description of the generation of the moving tubular electric field traps above this particular chip is given elsewhere (*4*, *8*); a pictorial representation of the tubular traps above the chip, indicated in blue, is shown in the lower panel of Fig. 1.

The experiments here were performed with CO molecules in the low-field–seeking levels of the metastable $a^3\Pi_1$ ($v' = 0, J' = 1$) state. For these molecules, the electric field minima correspond to traps with a depth of about 50 mK when a constant frequency ν is applied. When the frequency ν is changed linearly in time, i.e., when a constant acceleration is applied, the diameter and depth of the traps decrease but three-dimensional confinement is maintained up to an acceleration of about 1.5×10^6 m/s^2. In the low–electric field region around the long axis of the trap, molecules can be lost due to nonadiabatic transitions to nontrappable degenerate states (*9*). In magnetic traps for atoms on a chip, this hole at the center of the trap is commonly plugged by adding a homogeneous magnetic field. An offset magnetic field could also be added in the present setup. For molecules in electric traps, however, there often exists the unique alternative solution to simply select an isotopologue with a favorable hyperfine level structure such that there is no degeneracy between trappable and nontrappable states in zero electric field (*10*). The most abundant carbon monoxide isotopologue, $^{12}C^{16}O$, has no hyperfine structure, and the low-field–seeking $M\Omega = -1$ level of the $a^3\Pi_1$ ($v' = 0, J' = 1$) state is degenerate with the $M = 0$ level in zero electric field, making this species susceptible to nonadiabatic transitions. In $^{13}C^{16}O$, however, the coupling of the nuclear spin of the ^{13}C nucleus with the orbital angular momentum results in a lifting of this degeneracy. As shown in the inset of Fig. 2, the low-field–seeking

Fritz-Haber-Institut der Max-Planck-Gesellschaft, Faradayweg 4-6, D-14195 Berlin, Germany.

*To whom correspondence should be addressed. E-mail: meijer@fhi-berlin.mpg.de

levels never come closer to the nontrappable level than 53 MHz in any electric field for ^{13}CO (*11*), effectively preventing nonadiabatic transitions from occurring.

In Fig. 2, the measured arrival-time distributions of metastable ^{13}CO molecules are shown for four different sets of wave forms of the potentials applied to the chip. When the molecules with an initial velocity of 312 m/s have just arrived above the chip, the external potentials are switched on. When wave forms with a constant frequency of ν = 2.6 MHz are used, the traps move at a constant velocity of 312 m/s while transporting the molecules to the other end of the chip. The total time that it takes the molecules to travel the complete 30-cm distance from the excitation point to the detector is about 0.96 ms in that case. With increasing accelerations, the molecules are slowed down from their initial velocity of 312 m/s to the indicated final velocities of 240, 168, or 96 m/s and arrive ever later on the detector. The broad background that is observed at early times results from metastable CO molecules in the $M = 0$ level that are hardly influenced by the electric fields. For comparison, the results for the guiding at 312 m/s and for the gentle deceleration of ^{12}CO molecules to 240 m/s are shown on the same scale as well (in gray). The dramatic loss in signal when going from ^{13}CO to ^{12}CO indicates the importance of nonadiabatic transitions even during the less than 200-μs residence time of the molecules in the electric field traps. All other experiments have therefore been performed with ^{13}CO.

In Fig. 3, measurements are shown to demonstrate how the longitudinal phase-space distribution of the ^{13}CO molecules can be manipulated in a three-step process to achieve both the maximum number of trapped molecules on the chip and the optimum detection sensitivity. In the inset, the corresponding longitudinal phase-space distributions are given at eight different times (A to H). Distribution (A) depicts the initial 1-mm-long distribution directly after laser excitation, just before the skimmer, whereas (B) is the same distribution after 0.6 ms of free flight. First, for optimum loading on the chip, a velocity-focusing deceleration is applied to sweep the velocities of all molecules of the incoming beam together (B to D). An array of about 250 electric field traps is loaded on the chip, one after the other, in this way. Second, a rapid deceleration is applied to bring all these traps to the desired final velocity on the chip (D to E). The chosen final velocity is 180 m/s in this particular measurement, but could be tuned to any velocity, including standstill. Third, for optimum detection of the molecules, a space-focusing acceleration is applied (E to G) to eject the molecules off the chip with velocities such that they all arrive at the same time on the detector (H), irrespective of their original position on the chip. The required values for the velocity-focusing deceleration and the space-focusing acceleration are determined by the geometry of the experimental setup. The gray curve in Fig. 3 is the measurement when the time sequence (A to E) is as described here, but when no acceleration is applied to eject the molecules off the chip. Despite the narrow velocity distribution achieved for the trapped molecules, the range of distances from the detector they exhibit leads to a broad distribution of arrival times (H′). The black curve is obtained when the optimum loading and detection strategy (A to H) is used.

The observed integrated signal intensity of the measurements shown in Fig. 3 is about 25 counts per pulse. As it is estimated that about one count is obtained for every hundred metastable CO molecules that hit the detector, this integrated value implies that there are ~10 CO molecules per electric field trap on the chip. The density in the traps is thus on the order of 10^7 molecules/cm^3, similar to the densities that have been obtained in macroscopic traps after beam deceleration (*7*). This density is given by the original density in the molecular beam at the entrance of the chip and can be several orders of magnitude higher when more intense pulsed sources are used or when the chip is brought closer to the beam source; the latter can readily be done with the chip but is less straightforward for larger-scale decelerators. The total volume of the simultaneously loaded tubular traps on the chip is ~0.25 mm^3, which is only between one and two orders of magnitude less than the volume of the typical macroscopic electrostatic traps that have been used thus far (*7*). The ejection of the molecules off the chip and their spatial focusing further downstream is ideal for any laser-based

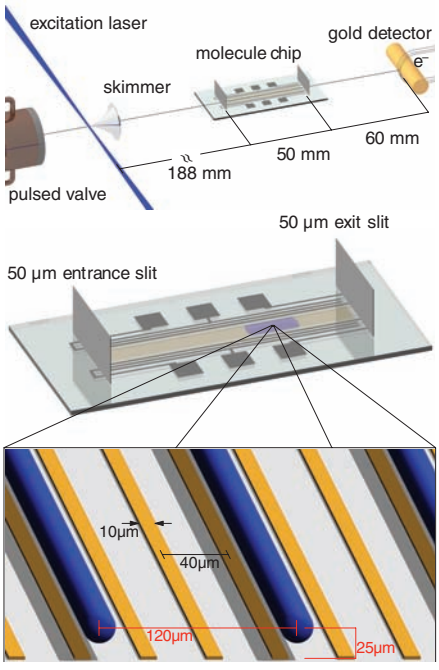

Fig. 1. Schematic of the experimental setup with an enlarged view of the chip. A pulsed beam (10 Hz) of ground-state CO molecules with a mean velocity of about 310 m/s is produced by expanding a mixture of 20% CO in krypton through a cooled valve in vacuum. Just before passing through the skimmer, CO molecules are prepared in the upper Λ-doublet level of the $a^3\Pi_1$ ($v' = 0$, $J' = 1$) state by direct laser excitation from the electronic ground state. The pulsed laser (5-ns pulse) is weakly focused (1-mm diameter) onto the molecular beam, creating a well-defined packet of metastable CO molecules. About 19 cm downstream from the laser excitation point, the molecules pass through a 50-μm-high entrance slit and then travel closely above the chip over its full 5-cm length. At the end of the chip, the molecules have to pass through another 50-μm-high exit slit to then fly freely to a gold surface that is positioned 6 cm further downstream. The arrival-time distribution of the molecules on the gold surface is measured via recording of the Auger electrons that are emitted when the metastable CO molecules impact there.

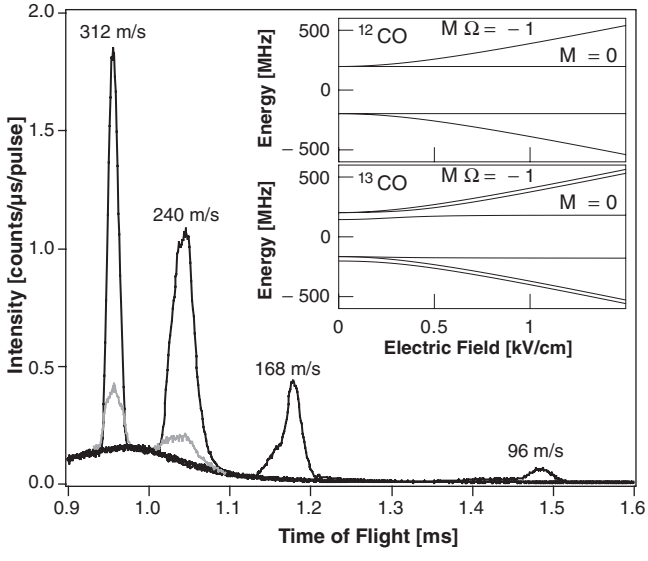

Fig. 2. Arrival-time distributions of ^{13}CO (black curves) and ^{12}CO (gray curves) molecules on the detector. The time scale is relative to the time of laser excitation, and the vertical scale is in counts per microsecond and per pulse. The initial frequency of the wave forms is 2.6 MHz in all cases, and this frequency is either kept constant or ramped down linearly in time while the molecules are above the chip. Ramping down to a final frequency of 2.0, 1.4, and 0.8 MHz results in final velocities of 240, 168, and 96 m/s and corresponds to accelerations of 0.40×10^6, 0.70×10^6, and 0.89×10^6 m/s^2, respectively. Each measured trace is averaged over 2 hours (at 10 Hz). (**Inset**) The levels of the $a^3\Pi_1$ ($v' = 0$, $J' = 1$) state of ^{12}CO and ^{13}CO, calculated from spectroscopic data (*11*), are shown in low electric fields.

detection scheme. When resonant laser ionization in combination with mass-selective ion detection is being used, the overall detection efficiency can approach unity. This makes the method outlined here applicable to a wide variety of molecules like (various isotopologues of) the hydroxyl radical, ammonia, water, and formaldehyde. All these molecules can be decelerated and trapped in their electronic ground state, in ro-vibrational levels that are well populated in a molecular beam, and for which sensitive laser-based detection schemes are available (*12*). To more generally prevent losses due to nonadiabatic transitions in these molecules, an offset magnetic field, directed parallel to the long axis of the trap and thereby always perpendicular to the electric fields above the chip, might be required.

In Fig. 4, a series of arrival-time measurements is shown that has been recorded after the ^{13}CO molecules have been held for certain times in stationary electrostatic traps on the chip. An important advantage of the present scheme is that the loading of stationary traps on the chip involves simply bringing already existing, fast-moving traps to a standstill. This is fundamentally different from trap-loading schemes using conventional Stark decelerators (*7*) because the effective traps that are present in those decelerators disappear at low velocities. In the measurements shown in Fig. 4, an array of about 60 electric field traps has been loaded and brought to a stop. After a variable holding time in the 0- to 2.5-ms range, these traps have been accelerated again and the molecules have been space-focused on the detector. In the inset, the integrated signal intensity is shown as a function of the holding time. The observed decrease of the signal as a function of time is consistent with the expected decay based on the known 2.6-ms lifetime of the $a^3\Pi_1$ ($v' = 0, J' = 1$) state of CO (*13*). Clearly, measurements like the one shown in Fig. 4 can be used to determine lifetimes of molecules in long-lived electronically or vibrationally excited states, something that is notoriously difficult to do without trapping and for which thus far large experimental machines had to be constructed (*13*–*15*). The presently achieved densities of the molecules on the chip are in principle already sufficient for this (one actually does not want the densities to be too high, to prevent collisions between the trapped molecules), but for accurate measurements the statistics still need to be improved to some degree, either by increasing the density or implementing more sensitive ionization detection schemes.

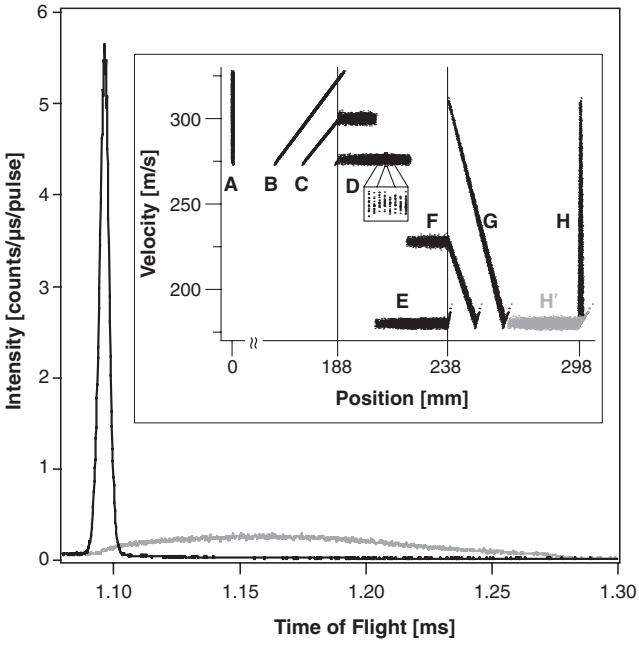

Fig. 3. Arrival-time distribution of ^{13}CO molecules ejected from about 250 simultaneously loaded electric field traps on the chip, both with (black curve) and without (gray curve) space focusing them on the detector. The time scale is relative to the time of laser excitation, and the vertical scale is in counts per microsecond and per pulse. Each measured trace is averaged over 2 hours (at 10 Hz). (**Inset**) The corresponding longitudinal phase-space distributions are shown at eight different times in the loading and detection cycle (A to H). By using a velocity-focusing deceleration of about 0.5×10^6 m/s^2 (B to D) followed by a rapid further deceleration of 1.20×10^6 m/s^2 (D and E), the molecules are brought to a velocity of 180 m/s on the chip. The edges of the chip are 188 and 238 mm away from the excitation point, indicated by vertical lines. An expanded view of the phase-space distribution at time (D), in which the individual electric field traps can be recognized, is shown as well.

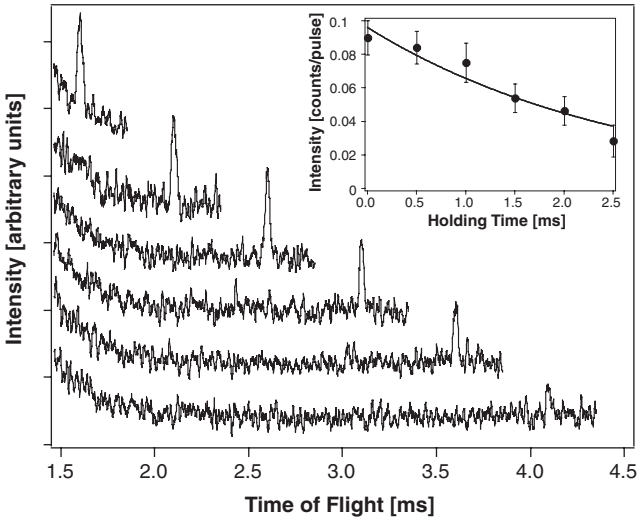

Fig. 4. Arrival-time distribution of ^{13}CO molecules ejected from about 60 simultaneously loaded stationary electric field traps on the chip after holding times ranging from 0 to 2.5 ms, in steps of 0.5 ms (from top to bottom). In these measurements, space focusing on the detector is used. The horizontal scale is relative to the time of laser excitation, and the curves have been given a vertical offset for clarity. Each measured trace is averaged over 4 hours (at 10 Hz). (**Inset**) The integrated intensity of the signal in counts per pulse is shown as a function of holding time, together with the expected dependence when only the phosphorescent decay of the metastable molecules is taken into account (*13*). The indicated error bars are determined from the 2σ noise on the baseline of the individual traces.

Many of the advances that were foreseen for microscopic magnetic traps for neutral atoms (*16*) and integrated atom optics on a chip (*17*) about a decade ago have now become a reality. The decisive advantage of the versatility of the lithographic wire structures can also be exploited for molecules. The ability of a molecule to rotate and vibrate allows for coupling to photons over an enormous range of frequencies. Coupling at microwave frequencies, in particular, provides a convenient interface between quantum optic and solid-state technologies (*6*). The use of miniaturized traps with inherent high trapping frequencies brings quantum degeneracy for samples of polar molecules considerably closer. A tight trap permits fast adiabatic changes of the confining potential, and via compression of a cloud of trapped molecules, increased thermalization rates and shortened times for forced evaporative cooling can be achieved. Here, we have experimentally demonstrated an integrated experimental approach to confine molecules in miniaturized traps on a chip and subsequently detect them, thereby opening up these fascinating research possibilities.

References and Notes

1. J. Fortágh, C. Zimmermann, *Rev. Mod. Phys.* **79**, 235 (2007).
2. W. Hänsel, P. Hommelhoff, T. W. Hänsch, J. Reichel, *Nature* **413**, 498 (2001).
3. T. Schumm *et al.*, *Nat. Physics* **1**, 57 (2005).
4. S. A. Meek, H. L. Bethlem, H. Conrad, G. Meijer, *Phys. Rev. Lett.* **100**, 153003 (2008).
5. D. DeMille, *Phys. Rev. Lett.* **88**, 067901 (2002).
6. A. André *et al.*, *Nat. Physics* **2**, 636 (2006).
7. S. Y. T. van de Meerakker, H. L. Bethlem, G. Meijer, *Nat. Physics* **4**, 595 (2008).
8. S. A. Meek, H. Conrad, G. Meijer, *N. J. Phys.* **11**, 055024 (2009).
9. M. Lara, B. L. Lev, J. L. Bohn, *Phys. Rev. A* **78**, 033433 (2008).
10. M. Kirste, B. G. Sartakov, M. Schnell, G. Meijer, *Phys. Rev. A* **79**, 051401(R) (2009).

11. R. H. Gammon, R. C. Stern, M. E. Lesk, B. G. Wicke, W. Klemperer, *J. Chem. Phys.* **54**, 2136 (1971).
12. The advantage of using metastable CO in the present experiments is that these molecules are prepared with a pulsed laser at a well-defined time and at a well-defined position in a single quantum state with the appropriate Stark shift. By detecting the Auger electrons when the metastable CO molecules impact on the Au surface, the full arrival-time distribution of the molecules can be recorded in a single pulse, and the schemes to manipulate the longitudinal phase-space distribution demonstrated in Fig. 3, for instance, can be rapidly tested and optimized. Even though the detection efficiency for metastable CO is not as good now as it can be for ionization detection, the multiplex nature of the trap-loading and detection scheme already enables us to detect down to one metastable CO molecule per hundred traps on the chip.
13. J. J. Gilijamse *et al.*, *J. Chem. Phys.* **127**, 221102 (2007).
14. S. Y. T. van de Meerakker, N. Vanhaecke, M. P. J. van der Loo, G. C. Groenenboom, G. Meijer, *Phys. Rev. Lett.* **95**, 013003 (2005).
15. W. C. Campbell, G. C. Groenenboom, H.-I. Lu, E. Tsikata, J. M. Doyle, *Phys. Rev. Lett.* **100**, 083003 (2008).
16. J. D. Weinstein, K. G. Libbrecht, *Phys. Rev. A* **52**, 4004 (1995).
17. E. A. Hinds, I. G. Hughes, *J. Phys. D Appl. Phys.* **32**, R119 (1999).
18. We acknowledge the help of B. G. Sartakov in the calculation of the hyperfine structure of ^{13}CO and the design of the electronics by G. Heyne, V. Platschkowski, and T. Vetter. This work has been funded by the European Community's Seventh Framework Program FP7/2007-2013 under grant agreement 216 774.

27 March 2009; accepted 26 May 2009
10.1126/science.1175975

Amplified Trace Gas Removal in the Troposphere

Andreas Hofzumahaus,[1] Franz Rohrer,[1]* Keding Lu,[1,2] Birger Bohn,[1] Theo Brauers,[1] Chih-Chung Chang,[3] Hendrik Fuchs,[1] Frank Holland,[1] Kazuyuki Kita,[4] Yutaka Kondo,[5] Xin Li,[1,2] Shengrong Lou,[1,6] Min Shao,[2] Limin Zeng,[2] Andreas Wahner,[1] Yuanhang Zhang[2]*

The degradation of trace gases and pollutants in the troposphere is dominated by their reaction with hydroxyl radicals (OH). The importance of OH rests on its high reactivity, its ubiquitous photochemical production in the sunlit atmosphere, and most importantly on its regeneration in the oxidation chain of the trace gases. In the current understanding, the recycling of OH proceeds through HO_2 reacting with NO, thereby forming ozone. A recent field campaign in the Pearl River Delta, China, quantified tropospheric OH and HO_2 concentrations and turnover rates by direct measurements. We report that concentrations of OH were three to five times greater than expected, and we propose the existence of a pathway for the regeneration of OH independent of NO, which amplifies the degradation of pollutants without producing ozone.

The central role of hydroxyl radicals (OH) in atmospheric chemistry was recognized by Levy in the early 1970s (*1*). Since then it has become more and more evident how OH radicals govern the degradation processes of air pollutants. OH radicals are short-lived (<1 s), and their formation and loss must be essentially balanced. OH is primarily formed through the photolysis of ozone, nitrous acid, and hydrogen peroxide and is consumed by a multitude of reactions with trace gases that can be oxidized. In this way, OH controls the removal of most atmospheric pollutants such as carbon monoxide (CO) and volatile organic compounds (VOCs). The OH reactions with CO and VOCs produce hydroperoxy (HO_2) and organic peroxy (RO_2) radicals, respectively. In continental air, with nitrogen oxides (NO_x) present, RO_2 is converted to HO_2 through reaction with NO. HO_2 further reacts with NO, thereby recycling OH. The ultimate loss of OH is the reaction with NO_2, forming nitric acid. These are the key processes that are believed to determine the self-cleaning ability of the troposphere (*2*, *3*). OH recycling enhances the efficiency of atmospheric oxidation, even at moderate NO concentrations. As a side effect, reactions of HO_2 or RO_2 with NO form NO_2, which produces ozone upon photolysis. This is the generally accepted, exclusive mechanism for the photochemical formation of ozone in the troposphere (*4*). OH formation through photolysis, HO_2 to OH recycling with NO, and OH loss with NO_2 have been established through a small number of well-understood reactions. In contrast, OH reactions with VOCs and the subsequent organic radical reactions are diverse and introduce enormous complexity into tropospheric chemistry, which is far from being fully explored (*5*, *6*).

The current understanding of tropospheric OH chemistry has been tested in a number of field campaigns, where the concentrations of OH and trace gases and meteorological parameters were observed simultaneously (*7*). However, OH observations are still too sparse, owing to the difficulty of measuring its extremely small and highly variable concentration, to provide a conclusive picture of the photochemistry in the entire troposphere (*8*–*10*). More experimental studies in different chemical environments are necessary to explore the various factors influencing the self-cleaning capability of the atmosphere. In this paper, we present concentration measurements of OH and HO_2 radicals in China (*11*), together with simultaneously measured mixing ratios of atmospheric trace gases and photolysis frequencies (*12*) (fig. S1). Complementary to direct measurements of VOCs, we also measured the total OH reactivity, k'_{OH}, corresponding to the inverse chemical lifetime of OH (*13*, *14*). Our measurements were part of an intense field campaign in a rural area, about 60 km NW of Guangzhou City, in the heavily populated Pearl River Delta (PRD) (*12*).

The diurnal dependences of the measured OH and HO_2 concentrations and k'_{OH} are shown

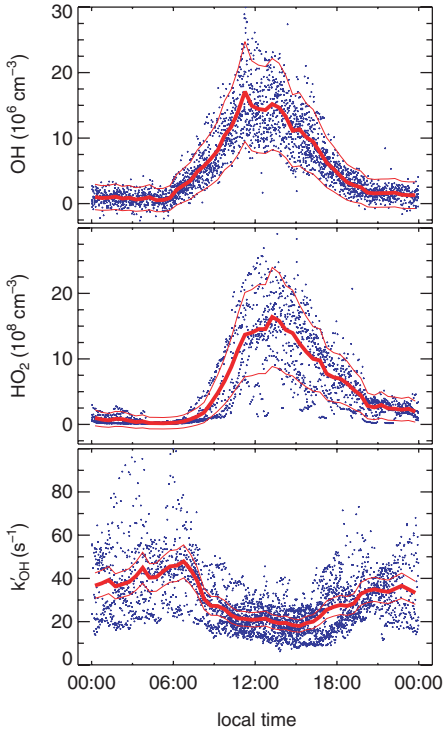

Fig. 1. Diurnal variation of OH, HO_2, and k'_{OH} near Guangzhou in the PRD, China, between 5 and 25 July 2006. Blue symbols denote individual data, and the thick red line the half-hourly mean diurnal profile. The enclosing thin red lines represent the maximum data variability caused by the measurement instrument (about 46% at noon), calculated as the sum of the 2σ measurement precision and the 2σ variability of its calibration. Campaign average calibration factors were used to convert measured OH and HO_2 signals into ambient concentrations.

[1]Forschungszentrum Jülich, Institut für Chemie und Dynamik der Geosphäre–2: Troposphäre, 52425 Jülich, Germany. [2]College of Environmental Sciences and Engineering, Peking University, Beijing 100871, China. [3]Research Center for Environmental Changes, Academic Sinica, Taipei, China. [4]Faculty of Science, Ibaraki University, Ibaraki 310-8512, Japan. [5]Research Center for Advanced Science and Technology, University of Tokyo, Tokyo 153-8904, Japan. [6]School of Environmental Science and Technology, Shanghai Jiaotong University, Shanghai 200240, China.

*To whom correspondence should be addressed. E-mail: f.rohrer@fz-juelich.de (F.R.); yhzhang@pku.edu.cn (Y.Z.)